Observation of Damage Accumulation under In-plane Shear Loading

C.Yilmaz[1,2,3], C. Akalin[2,3], I. Gunal[5], H. Celik[6], Murat Buyuk[2,3], A. Suleman[4*] and M. Yildiz[1,2,3]

[1]Faculty of Engineering and Natural Sciences, Sabanci University,
Tuzla, 34956, Istanbul,
TURKEY

[2]Integrated Manufacturing Technologies Research and Application Center, Sabanci University,
Tuzla, 34956, Istanbul,
TURKEY

[3]Composite Technologies Center of Excellence, Sabanci University-Kordsa, Istanbul Technology Development Zone,
Sanayi Mah. Teknopark Blvd. No: 1/1B, Pendik, 34906, Istanbul,
TURKEY

[4]Department of Mechanical Engineering, Center for Aerospace Research, University of Victoria,
Victoria, BC, V8W 3P6,
CANADA

[5]KNRTU-KAI named after A.N. TUPOLEV, Structural Strength Department,
Kazan,
RUSSIA

[6]Yonca-Onuk JV Shipyard, Tuzla, Istanbul,
TURKEY

* suleman@uvic.ca

ABSTRACT

Micro-damage initiation and accumulation in two different Glass Fiber Reinforced -E-glass and S-glass-Laminated Composite Structures (LCS) subjected to in-plane shear stressing were monitored with Acoustic Emission (AE) and thermography methods. AE signals caused by micro-damage formation were graphed as a scatter plot of Weighted Peak Frequency (WPF) versus Partial Power 2 (PP2) features and clustered using the K-means algorithm with Bray Curtis dissimilarity function thus resulting in three different well-separated clusters. Each of these clusters corresponds to different micro damages, i.e., transverse cracks, delaminations or fiber ruptures. It was observed that the E-glass reinforced LCS has higher numbers of AE hits. Thus, the total amount of micro-damage incurred as well as the average temperature change measured by thermography was higher for the E-glass reinforced LCS. It was shown that due to the curing induced residual tensile stress in E-glass reinforced LCS, the initial formation of delamination in E-glass reinforced LCS starts at higher load level. Under the applied shear load, a significant reduction in in-plane shear modulus was observed both for the E-glass and S-glass-reinforced LCS where the E-glass reinforced LCS shows greater reduction. The decrease in in-plane shear modulus was attributed to micro-damage accumulated in the LCS.

1.0 INTRODUCTION

The usage of LCSs has increased in engineering applications over the past decade, such as wind turbine blades, aircraft and naval components. The reason behind this increase was due to their high specific strength and stiffness compared to metallic materials. Moreover, LCS can be formed into complex shape and immune to corrosion. To be able to use LCSs in structural applications reliably without any abrupt failure, a detailed study on the reduction in engineering elastic constants of LCSs associated with micro-damage initiation and accumulation must be conducted. In literature, one may find several important studies on the micro-damage induced reduction in mechanical properties of LCSs under axial loading such as axial modulus and Poisson's ratio. For instance, Highsmith et al. [1] studied the effect of transverse crack on the axial stiffness reduction under the uniaxial quasi-static tension and tension-tension fatigue. The behaviour of Poisson's ratio under tensile loading was analyzed in references [2-6] wherein results indicated that formation of transverse crack causes apparent reduction in Poisson's ratio. Different sensor systems were also utilized to measure strain from the surface and interior of LCSs with the aim of calculating Poison's ratio reduction and studying the effect of sensor types on the Poisson's ratio measurement [7].

However, a few studies can be listed as to the reduction in in-plane shear modulus owing to the micro-damage initiation and accumulation under loading despite the fact that the in-plane shear modulus is among the very important mechanical properties, which is needed for predicting the structural response of LCSs under mechanical loading. Given that in-plane shear modulus can be measured with special fixtures such as Iosipescu shear fixture (ASTM D5379/D5379M – 12), in literature, research on shear loading mainly deals with addressing the drawbacks of the test fixture, the notch type of test specimens and the finite element analysis of test coupons [8-10]. Odegard et al. [11] compared the feasibility of Iosipescu test with 10^o off-axis test for measuring the in-plane shear modulus of unidirectional carbon fiber reinforced LCS and concluded that both tests yield a very similar value. Han et al. [12] evaluated the frame test with respect to the Iosipescu test, and deduced that the Iosipescu test delivers a more accurate result for shear properties of laminates than that of the frame test. Pierron et al. [13] addressed the reliability of in-plane shear strength measurement with the Iosipescu test and found that the shear strength measured by the Iosipescu shear test is smaller than the one determined by 10^o off-axis test. Sun et al. [14] investigated specimens with the V-notch and Round-notch in Iosipescu testing and arrived at a conclusion that Round-notch is more favourable. Tew et al. [9] studied the fixture and specimen interaction in the Iosipescu test and proposed two different types of fixtures, namely, pivoting and rounded load surface. Unlike the research in literature dedicated to determining optimum test specimen configuration, and to the investigation of test fixture and test type, there are limited number of studies which have addressed the evolution of the shear modulus reduction through using Iosipescu testing fixture. Salavatian et al. [15] considered the effect of transverse cracking on the reduction in in-plane shear modulus, excluding the possible effects of other micro-damage types such as delamination and fiber rupture among others. Salavatian et al. [16] also modelled the effect of internal frictions between the surfaces of transverse cracks on the reduction of in-plane shear modulus. Differently, Melin et al. [8] reported that the reduction in in-plane shear modulus is not due to the micro-damage (i.e., transverse cracking, delamination or fiber rupture) accumulation, rather, it is due to the viscous deformation and creep in the matrix phase.

To be able to understand the effect of micro-damage formation on the in-plane shear modulus of LCSs, in this study, acoustic emission (AE) method was used since it provides useful outputs that can be readily processed to distinguish possible damage generation mechanisms (fiber rupture, delamination, transverse cracking), which are particularly important for failure assessment of composite materials. AE technique uses piezo-electric sensors which are sensitive to short and weak transient waves released by micro-damage formation. Several studies have employed AE method during the tensile test of LCSs where transient waves generated by micro-damage formations are recorded and classified [17, 18]. A variety of classification procedures can be found in literature which use different features of waves such as rise time, peak amplitude, peak frequency and weighted peak frequency [19]. Among these features, the usage of weighted peak frequency (f_{wp}) with the unsupervised K-means algorithm is the most promising one.

In addition to AE method, due to the significance of the micro-damage formation on the mechanical properties of LCSs, several studies used the concept of thermography and measured surface temperature of composite specimens with an IR (infrared) camera to evaluate the damage state of LCS under fatigue loading. For example, Genest et al.[20] employed IR camera for detecting the disbonding area between a composite repair patch and aluminum host material under tension-tension fatigue. Liu et al. [21] proved that the thermography can be an effective way to determine the damage evaluation of carbon-fiber/SiC-matrix composites under the tension-tension fatigue. Naderi et al. [22] also showed that the thermography can be used to reveal the fatigue stages of glass/epoxy composite under bending fatigue. Montesano et al. [23] assessed the damage states of woven carbon fiber/epoxy composites with thermography subjected to uniaxial in-plane tensile quasi-static and fatigue loading. The thermography based damage monitoring and assessment is not limited to composites and have been used for metallic materials as well. For instance, Crupi [24] used IR camera to measure the surface temperature of steel and aluminum under high cycle fatigue and showed that the temperature increment as a result of the heat dissipation can be used as a life parameter. Fargione et al. [25] showed that temperature measured by the IR camera can reveal the damage state of steel and help the rapid determination of fatigue curve for steel.

Although, there are numerous studies on damage evaluation with AE method and thermography under different loading conditions (i.e., static and fatigue), and on the optimization of the shear testing of the composite, to the best of the authors' knowledge, there is no combined damage assessment study using AE and thermography methods to study the reduction in in-plane shear modulus of LCS under the shear loading. In this study, we have monitored the initialization and accumulation of different micro-damage types in two different LCS under shear loading, and investigated the effect of micro-damage on the shear modulus reduction. The LCSs were composed of S-glass and E-glass reinforcements. The micro-damage monitoring was accomplished by piezo electric sensors connected to the AE streaming hardware. The stress waves released by the micro-damage were converted to AE signals by piezo electronic sensors. Thereafter, a comprehensive classification of AE data was achieved by K-means algorithm which uses the Bray-Curtis dissimilarity function for assigning data points to the relevant cluster. Three different clusters were formed, which corresponds to transverse cracks, delaminations, and fiber ruptures. The temperature change on the surface of the specimens was monitored by the IR camera to associate the damage type and accumulation with temperature increase. The combined usage of AE and thermography in studying the behavior of LCSs under in plane shear loading enabled us to elucidate the effect of micro-damage initiation and accumulation on the shear properties as well as shear modulus reduction.

2.0 METHODOLOGY

2.1 Materials and Sample Preparation

Two different glass-fiber reinforcements (S-glass and E-glass woven rowing fabric with 600 gsm areal weight with epoxy vinyl ester compatible sizing agent) were purchased from Metyx, Turkey, and then used to manufacture composite plates through using vacuum infusion method. As a matrix material, a room temperature curing epoxy vinyl ester resin (Derakane 8084, Ashland Inc.) was chosen. Curing process lasted 12 hours at room temperature without post curing. The curing process of epoxy vinyl ester resin was exothermic, leading to a temperature increase up to 135 Celsius. The produced composite plates comprise 8 layers of glass-fabrics. The plates were cut with a water-cooled diamond saw in dimensions given in Figure 1 in accordance with ASTM D 5379 standard. Specimens had thickness in the range of 4.2 - 4.7 mm. The V-notch grooves were machined with vertical milling machine. Thereafter, sides of specimens were grinded and rosette type strain gages acquired from Micro Measurement with a code of CEA-06-187UV-350 were applied to the front surface of test specimens as seen in Figure 1. The fiber volume fraction for S-glass and E-glass reinforced LCS were measured to be 40 % and 42 %, respectively.

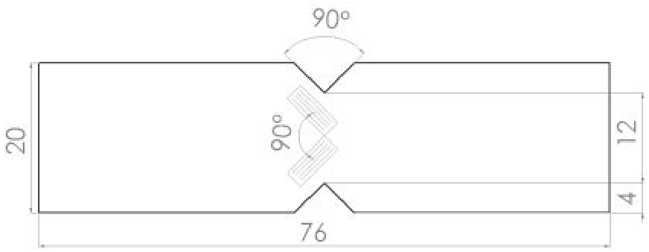

Figure 1: Dimensions of Iosipescu test specimen in mm.

2.2 Mechanical Testing

All in-plane shear tests were performed by using Instron 8801 UTM (Universal Testing Machine) combined with 8800MT digital controller. Instron 8801 UTM was equipped with a Dynacell load cell of ±100 kN. Specimens were installed into the Iosipescu test fixture installed on the lower jaws of the UTM. Thereafter, point contacts were attached to the test fixture to prevent the twisting and bending of test specimens. An Iosipescu fixture with V-notch shear specimen can be seen in Figure 2 (a). Strain-gage leads were mounted on electrical adapters connected to the strain channel on the test machine. A preload of 40 N was applied to all specimens to enable the proper contact of test apparatus with the load frame. In-plane shear test was performed under the constant crosshead-displacement of 2 mm/min. Bluehill 3 software was used to control the test machine as well as stress-strain data acquisition. Specimens were divided into two groups, namely, with and without a strain gage, because strain gage covers whole V-notch region thereby concealing the view of the IR camera. From each of two different LCSs, six specimens were tested, three of them were used in IR imaging and AE measurement, and remaining three were used in shear modulus measurement. To prevent Iosipescu shear fixture from getting damaged, all tests were terminated when the strain level of 2x104 $\mu\varepsilon$ was reached.

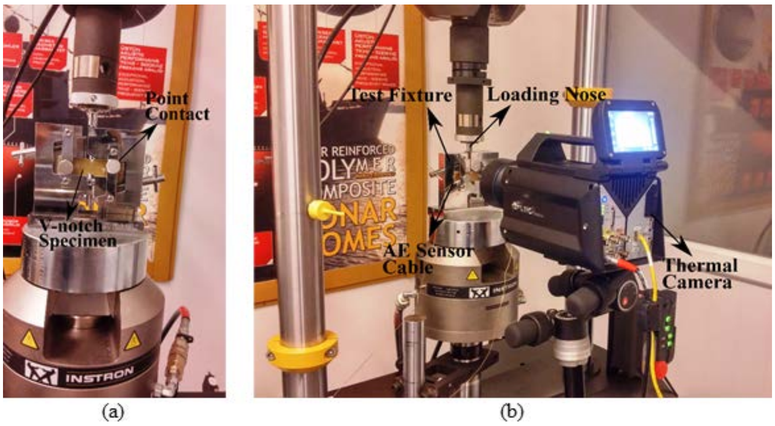

Figure 2: (a) A close-up view of Iosipescu test fixtures with V-notch specimen, (b) picture of experimental set-up.

2.3 Acoustic Emission and Thermography

All the elastic waves generated by micro-damages were detected by two wide-band (WD) piezo-electric sensors (PICO-200-750 kHz Lightweight Miniature AE Sensor, Mistras) bonded to the surface of specimens with a hot-melt adhesive. AE sensors were interrogated with the Mistras PCI- 2 AE setup equipped with Mistras 0/2/4 preamplifier. A 20-dB gain was utilized to amplify the signal output from WD piezo–electric sensors by tenfold. The signal acquisition threshold of 40 dB was implemented, thus eliminating the signals below this threshold. A comprehensive noise removal and feature extraction capabilities of Noesis software were employed to process AE waveforms. To eliminate the noise in the acquired signal, a Bessel band-pass filter of 10th order was applied to all the acquired waveforms. Band-pass filter range was set to 20-800 kHz to eliminate the signals with frequencies below 20 kHz and above 800 kHz. Signal based AE technique [26] was applied to each AE waveforms to extract features such as peak frequency (f_{peak}), frequency centroid ($f_{centroid}$), and partial power, among others. Here, f_{peak} is the frequency where power spectrum gets its maximum, $f_{centroid}$ is the sum of frequency times magnitude (amplitude of power spectrum at frequency f) divided by sum of magnitude, and partial power is defined as the percentage of energy available at a given frequency range in the power spectrum of the waveform as given in Figure 3. Two other important AE features are the weighted peak frequency (f_{wp}) and partial power 2 ($PP2$) where f_{wp} is calculated by using the following relation $f_{wp} = \sqrt{f_{centroid} * f_{peak}}$ and $PP2$ is determined by summing the power spectrum in the range of 250-450 kHz, which is divided by total power, and multiplied by 100. The $PP2$ and f_{wp} were used in the K-mean clustering to associate the waveforms with micro-damage types, namely, transverse crack, delamination or fiber rupture. When $PP2$ and f_{wp} were graphed as a scatter plot, three data groups were formed as seen in Figure 3, where each group corresponds a different micro-damage type (transverse crack, delamination and fiber rupture). An appropriate and reliable clustering algorithm is required to associate data points on transition zones or boundaries of data scatters to these groups correctly.

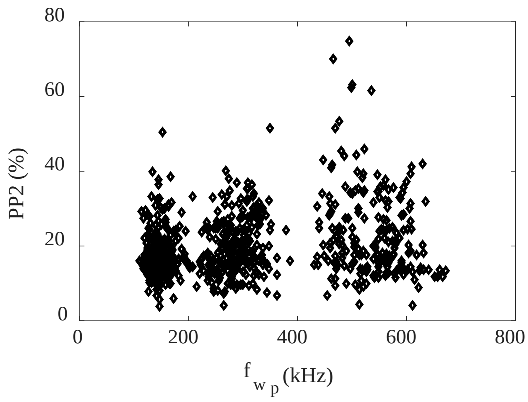

Figure 3: A representative f_{wp} versus $PP2$ scatter of a E-glass sample

For the classification, the hits (AE signals created by stress waves) only originated between two sensors were utilized. The classification of hits was performed by using an open-source software, Elki [27]. K-means algorithm with Bray-Curtis dissimilarity function was chosen to classify and relate the hits to the micro-damage types, i.e., a transverse crack, delamination or fiber rupture.

Surface temperatures of Iosipescu specimens were measured with an Infrared (IR) Camera model FLIR X6580sc. The IR camera with 50-mm lens was placed at approximately 40 cm away from the test specimens as shown Figure 2 (b) to obtain clear images. The IR camera was used in this study can measure temperature from $20^{\circ}C$ to $3000^{\circ}C$ with the reading accuracy of 1 %.

3.0 RESULTS AND DISCUSSION

3.1 Reduction in In-Plane Shear Modulus

Iosipescu shear test can provide the shear strength, shear modulus and shear strain of composite materials in different planes of interest. In this study, it was mainly used to monitor the variation of in-plane shear modulus of two different composite structures with E-glass and S-glass reinforcements under the shear loading. Figure 4 (a) and (b) respectively give in-plane shear stress-strain curves and the variation of normalized shear modulus for E-glass and S-glass reinforced LCS where G_{12}^{0} in the figure is the maximum value of shear modulus calculated from entire stress-strain data set.

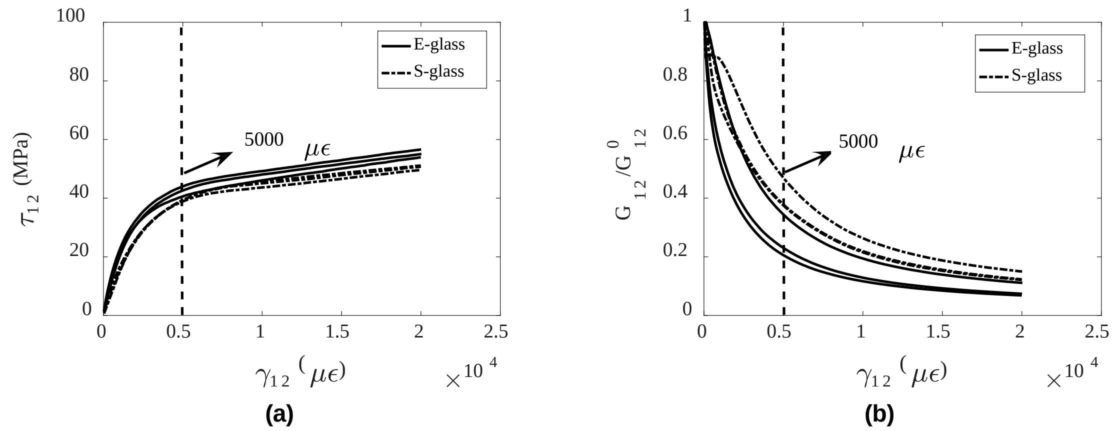

Figure 4: (a) In-plane shear stress-strain curves and (b) the variation of normalized shear modulus for E-glass and S-glass reinforced LCS.

The constituents of LCSs used in this study namely, fiber reinforcement (E-glass fibers and S-glass) and matrix (a thermosetting resin) materials have brittle failure mechanics. However, it is important to note that despite the brittle nature of the matrix and reinforcing materials, in-plane shear stress-strain diagrams of tested LCSs show a ductile-like behavior rather than a brittle-like one. The reason behind the ductile-like behavior was the high amount of deformation in the V-notch region compared to rest of specimens. As the load on the test sample increases, the V-notch region was populated by micro-damages (transverse cracks, delamination and fiber rupture), which grew in size and spread over the whole V-notch region. The formation and accumulation of micro-damages created a macroscopically visible damage zone (white colored V-notch region) as shown in Figure 5. Some cracks in this damage zone extended beyond V-notch region, which were marked by circles in Figure 5. When a micro-damage saturation point was reached (marked with the dashed vertical line in Figure 4 (a)), which means that whole V-notch region is covered by micro-damages as shown in Figure 5, LCS lost its load carrying capacity as can be inferred from Figure 4 (a) where the stress increases with a smaller slope after 5000 $\mu\varepsilon$ for both types of LCSs. The decrease in the slope of stress-strain curve marks the beginning of larger deformation due to the high damage density in the V-notch region where the material starts revealing a ductile-like behavior. The concentration of damage in a small area where the in-plane shear modulus was measured causes a significant amount of reduction in the in-plane shear modulus as can be seen in Figure 4 (b). Although both laminates showed nearly similar linear in-plane shear stress-strain behavior up to the 5000 $\mu\varepsilon$ (which is evident in Figure 4 (a)), the decrease in the shear modulus for the E-glass and S-glass reinforced LCS up to 5000 $\mu\varepsilon$ is notably different. The average reduction in in-plane shear modulus for S-glass and E-glass reinforced LCS is 60 % and 74 %, respectively as seen in Figure 4 (b). Besides, the shear modulus of E-glass reinforced LCSs reduces notably faster than that of S-glass reinforced LCSs, hence indicating that damage formation and accumulation is much easier in E-glass reinforced LCSs.

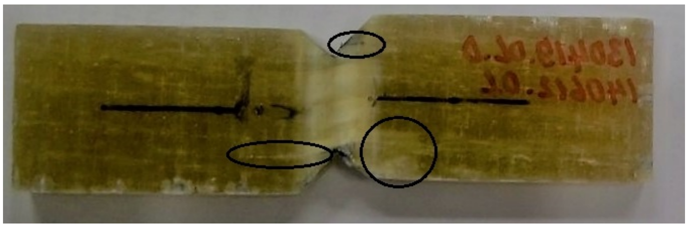

Figure 5: A tested Iosipescu shear specimen.

3.2 Acoustic Emission of Laminates

Here, we have presented the results of AE emission study on identifying and quantifying micro-damage initiation, total micro-damage accumulations, and the effect of different micro-damage types on the in-plane shear modulus of E-glass and S-glass fiber reinforced polymeric composites under the in-plane shear stress. The AE signals for two different laminates were clustered with K-means algorithm and representative results from each of the laminates are presented in Figure 6 (a) and (b). Knowing that each micro-damage type causes a signal with different f_{wp} such that low, moderate and high values of f_{wp} represent respectively transverse crack, delamination and fiber rupture [28, 29], the results given in Figure 6 (a) and (b) indicate three well-distributed signal clusters which can be associated with transverse crack, delamination, and fiber rupture.

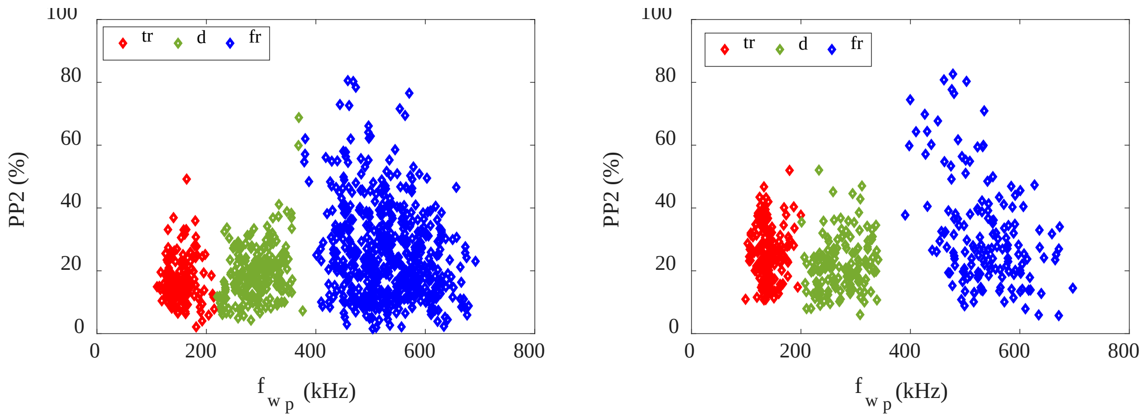

(a) **(b)**

Figure 6: Representative K-means clustering results for laminates with (a) E-glass and (b) S-glass reinforcements

To compare the average number of different hits in S-glass and E-glass reinforced LCSs, equation (1) is considered and results are presented in Figure 7 as a bar chart.

$$\hat{H}_t^s = \sum_{j=1}^{j=N} H_{t,j}^s / N \qquad (1)$$

where $H_{t,j}^s$ is the cumulative hit number of jth specimen that was calculated through summing all hits for the tth micro-damage type (micro-damage types are transverse crack, $t{=}tr$, delamination, $t = d$ and fiber rupture, $t = fr$) and N=3 is the total number of specimens considered. Here, the superscript "s" corresponds to reinforcement types in that $s =$ E-glass or S-glass. The average numbers of different hits in S-glass reinforced LCS are very close to each other with a minor difference with the following order of

$\hat{H}_{tr}^{E} > \hat{H}_{d}^{E} \geq \hat{H}_{fr}^{E}$ (Figure 7). Figure 7 also indicates that the total amount of AE hit in the E-glass reinforced LCS is higher than that of S-glass for all damage types thereby revealing that E-glass reinforced LCS is more prone to micro-damage accumulation. This result explains the reason behind larger drop in shear modulus of E-glass reinforced LCS in comparison to that of S-glass reinforced LCS under the in-plane shear loading. The accumulation of all micro-damage such as fiber rupture, delamination, and transverse crack preclude the load transfer in the shear plane hence leading to the reduction in in-plane shear modulus.

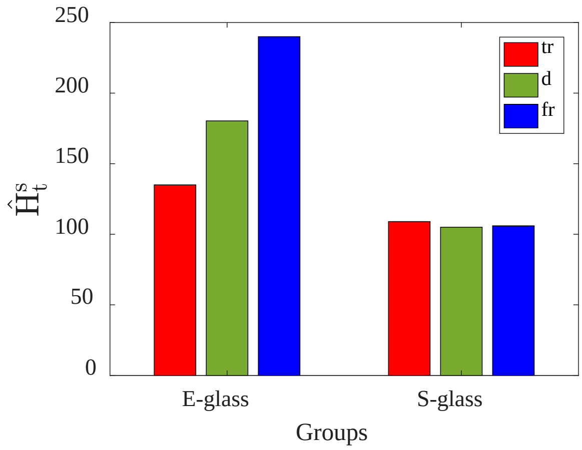

Figure 7: Average number of different signal types recorded in S-glass and E-glass reinforced

Another important parameter analyzed in this study was the damage initiation in LCSs under in-plane shear loading. The damage initiation was characterized by an onset ratio, which is defined as the ratio of stress at which the first micro-damage signal appears to the final stress at which test is stopped (the strain level of 2×10^4 με). The onset ratios for different micro-damage types are tabulated in *Table 1*.

Table 1: Onset ratio of micro-damage for E-glass and S-glass reinforced LCSs.

Type of LCS	σ_{otr}	σ_{od}	σ_{ofr}
S-glass reinforced	0.055	0.055	0.234
E-glass reinforced	0.052	0.072	0.083

The onset ratio of transverse crack (σ_{otr}) and fiber rupture (σ_{ofr}) for the E-glass reinforced LCS is smaller than that for the S-glass reinforced LCS whereas the onset ratio of delamination (σ_{od}) for the S-glass reinforced LCS is bigger than that for E-glass-reinforced LCS. The lower values of σ_{otr} and σ_{ofr} for E-glass reinforced LCS clearly suggests that the E-glass reinforced LCS is more vulnerable to transverse crack and fiber rupture formation than S-glass under in-plane shear stress loading, but less prone to delamination in comparison to S-glass reinforced LCS. Table 1 evidently shows that in the E-glass reinforced LCS, the deformation starts with the formation of transverse cracks which are perpendicular to loading direction. The transverse cracks in a small V-notch region coalesce hence leading to the occurrence of delamination and subsequently fiber rupture due to the fact that the load carrying capacity of the matrix is lessened owing to the transverse crack and delamination, as depicted in Figure 8 (a). On the other hand, as for the S-glass reinforced LCS, the deformation in V-notch region begins with the creation of transverse crack and delamination simultaneously under the same stress level, which is followed by fiber ruptures, as schematically described in Figure 8 (b).

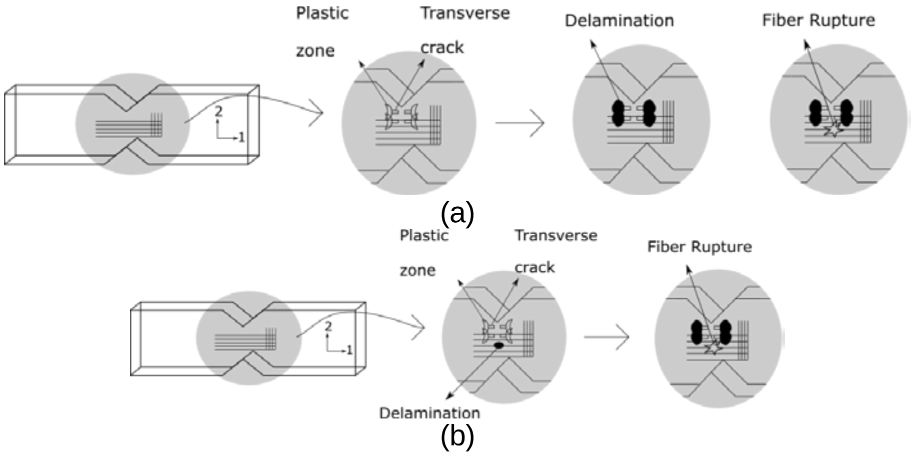

Figure 8: A schematic illustration of micro-crack initiation in a) E-glass and b) S-glass reinforced LCSs.

3.3 Surface Temperature Monitoring

Figure 9 (a)-(h) shows temperature map of a specimen attached to the Iosipescu fixture during the shear test. Before loading the specimen, there was a significant temperature gradient on the surface of the specimen as seen in Figure 9 (a). This temperature gradient was due to the fact that the lower part of the specimen directly touched the metal surface of the Iosipescu test fixture which was in contact with the rest of the UTM machine that acted like heat sink, thereby causing low temperature profile at the bottom portion of the specimen. Upon loading the specimen, micro-damage predominantly occurs in the V-notch region due to the stress concentration, leading to a temperature rise. The temperature rise can be related to several combined reasons such as heat generation due to the plastic deformation at the tips of cracks formed, and the friction between the internal surfaces of the cracks [30]. Referring to temperature variation in Figure 9, one can observe that the micro-damage starts in the upper V-notch as a thin spike and extends across the lower V-notch in a direction parallel to the applied load. As more micro-damage accumulates, the temperature of the mid-section of the specimen raises. To be able to monitor the evaluation of average temperature in the vicinity of V-notch region for each specimen, a rectangular domain with the dimensions of 4x10 mm was considered on the recorded images as shown in Figure 9. The calculated average temperatures for all specimens were plotted as a function of shear stress in Figure 10. The S-glass reinforced LCS shows negligible temperature change up to 45 MPa (Figure 9 and Figure 10), after which a significant rise was observed until fracture. On the other hand, temperature monotonically increased for the E-glass reinforced LCS and, at the end of the test, E-glass reinforced LCS had higher values of temperature than the S-glass reinforced LCS, attributable to larger micro-damage accumulation in E-glass reinforced LCS. This observation coincided with the results of AE for E-glass reinforced LCS..

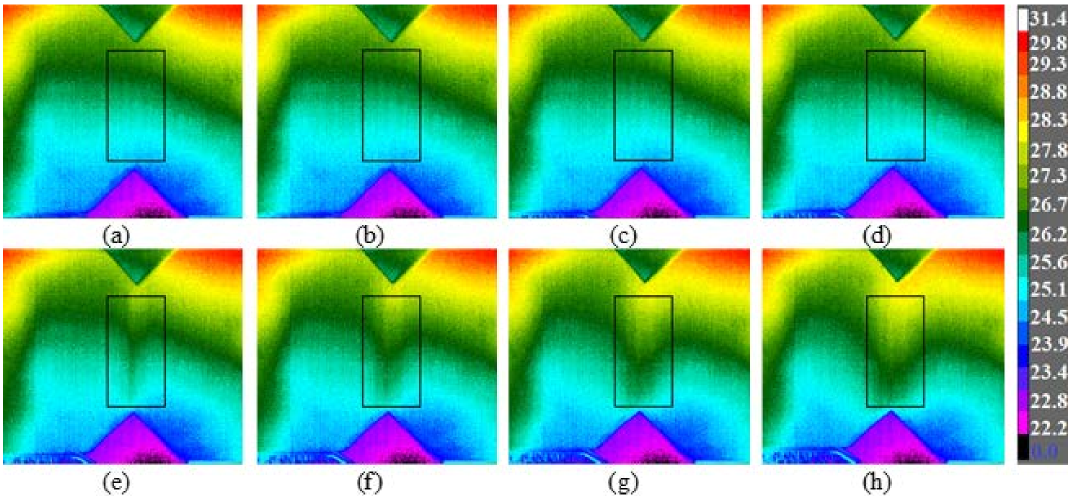

Figure 9: Temperature map of an S-glass reinforced Iosipescu specimen in the V-notch region during the shear test. Images are taken at the following stress levels; a) 0 MPA, b) 15 MPa, c)30 MPa, d) 43 MPa, e) 47 MPa, f) 50 MPa, g)52 MPa, h) 55 MPa

The inset figures a, b and c in Figure 10 indicate the cumulative number of hits corresponding to shear stress ranges of 0-20 MPa, 20-40 MPa and after 40 MPa where the letters E and S, respectively, show the results for E-and S-glass reinforced laminates for three different damage types, i.e., transverse crack, delamination, and fiber rupture. It is seen that at the initial state of the loading between 0-20 MPa, the occurrence of transverse crack and delamination for S-glass LCS is higher than that for E-glass. There might be two possible physical reasons that can be referred to for explaining why transverse cracks and delamination in S-glass reinforced LCS is higher than that in E-glass reinforced LCS. The first one is related to the strength of the S-glass while the second one is associated with the residual stress. Knowing that S-glass is of a notably higher tensile stress and modules values than E-glass [31], it is logical to expect that the S-glass reinforced LCS is much more stiffer or has a brittle nature, which is expected to be much prone to transverse crack formation and delamination promoted by the coalescence of transverse cracks. Therefore, at initial loading state up to 20 MPa, the cumulative number of hits for both transverse cracks and delamination in S-glass fiber reinforced LCS is larger than that in E-glass fiber reinforced LCS. In relation to the second reasoning, the coefficient of thermal expansion (CTE) of E-glass is nearly 3.5 times larger than that of S-glass [31]. In the curing process of composites, naturally, E-glass will expand more in comparison to S-glass, and upon curing of the epoxy resin which locks the expanded length of the fibers, E-glass reinforced LCS will experience a larger residual tensile stress than that of S-glass reinforced LCS. The residual tensile stress will act as a crack closure force since it is in the length direction of transverse cracks. As result, the crack coalescence in E-glass reinforced LCS is expected to be more difficult than that in S-glass reinforced LCS. Therefore, transverse cracks formed in S-glass reinforced LCS can relatively easily coalesce thereby promoting the occurrence of delamination, which explains why at initial loading the cumulative number of hit pertaining to delamination for S-glass reinforced LCS is higher than that of E-glass reinforced LCS.

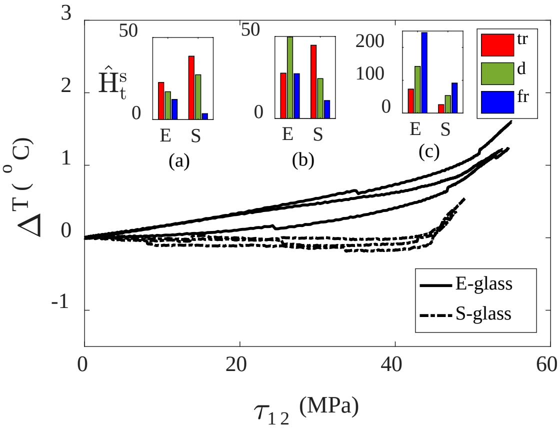

Figure 10: The average temperature change of LCSs with respect to the in-plane shear stress.

In comparing results for E-glass reinforced LCS in inset figures a, b and c, one can see that as the applied shear stress increases referring to the inset figure b, naturally, existing damages coalesce thereby promoting delamination and facilitate the formation of new transverse cracks and delaminations. Since the load carrying capacity of matrix is lessened due to matrix damages with the increase of the applied shear stress, E-glass fibers in the LCS will be carrying the larger portion of the applied load with its lower fiber strength and modulus compared to S-glass, hence experiencing more rupture than S-glass.

Upon comparing inset figures, a and b, for S-glass fiber reinforced LCS, it is seen that the transverse cracks and delamination are not intensified with the increase in applied shear stress in comparison to E-glass reinforced LCS. This is due to the fact that S-glass fiber does not rupture easily and in turn carries larger portion of the applied load. With the increase in applied shear stress, the load carrying capacity of matrix material is lessened due to matrix damage formation, and naturally S-glass fibers carry larger portion of the applied load, hence leading to an increase in the fiber rupture. After 40 MPa, since the matrix is weakened totally, the applied load is embraced mainly by the fibers. Therefore, there is obvious increase in the cumulative number of hits relevant to fiber rupture.

The thermal conductivity of S-glass is higher than that of E-glass, being respectively, 1.45 W/m•K, and 1.3 W/m•K at room temperature [31]. Therefore, the heat generated by transverse cracks and delamination in S-glass reinforced LCS can be transferred to ambient environment as well as Iosipescu test fixture faster than E-glass reinforced LCS. Therefore, the temperature rise in S-glass reinforced LCS is smaller than that in E-glass reinforced LCS. It is seen from the inset figure c that after nearly 40 MPa, the fiber fracture becomes dominantly higher than both transverse cracks and delamination for both E-and S-glass reinforced CLSs. The sudden rise in temperature clearly indicates that fiber rupture generates more heat than what transverse cracks and delamination leads to.

4.0 CONCLUSION

The aim of this study was to compare to damage initiation and accumulation behavior of E-glass and S-glass reinforced LCS under the shear loading. For this purpose, the surface temperature and AE hits of the S-glass and E-glass reinforced LCS specimens were recorded under in-plane shear loading. The in-plane shear stress was applied to V-notch specimens with the Iosipescu test fixture. AE signals were clustered with K-means algorithm and three well-separated clusters were obtained. Each of clusters contain AE signal belong to different micro-damage types namely, transverse crack, delamination, and fiber rupture. Following conclusions were drawn from this study:

AE signals can be successfully clustered with K-means algorithm by using Bray-Curtis dissimilarity function.

The tensile residual stress in E-glass reinforced LCS delay the coalescence of transverse crack and in turn delamination. Hence, the onset ratio of delamination in S-glass reinforced LCS is smaller than in E-glass reinforced LCS.

1. In total, a larger amount of micro-damage occurs in the E-glass reinforced LCS than S-glass reinforced LCS.

2. It is shown that there is an obvious connection between the total number of AE hits, rise in temperature and decrease in in-plane shear modulus. The larger the drop in in-plane shear modulus, the higher the number of AE hit and temperature rise of the tested specimen.

ACKNOWLEDGEMENT

The authors gratefully acknowledge the funding provided by Ministry of Science, Industry and Technology of Turkey for the project with the contract number of 01307.STZ.2012-1. The first author also gratefully acknowledge the funding provided by The Scientific and Technological Research Council of Turkey (TUBITAK) under the 2214-A International Research Fellowship Program for PhD Students.

5.0 REFERENCES

1. Highsmith A.L. and Reifsnider K.L. (1982) Stiffness-reduction mechanisms in composite laminates. *Damage in composite materials* **775**: 103-117.
2. Gao F., Boniface L., Ogin S., Smith P. and Greaves R. (1999) Damage accumulation in woven-fabric CFRP laminates under tensile loading: Part 1. Observations of damage accumulation. *Composites science and technology* **59**: 123-136.
3. Smith P.A. and Wood J.R. (1990) Poisson's ratio as a damage parameter in the static tensile loading of simple crossply laminates. *Composites Science and Technology* **38**: 85-93.
4. Surgeon M., Vanswijgenhoven E., Wevers M. and Van der Biest O. (1999) Transverse cracking and Poisson's ratio reduction in cross-ply carbon fibre-reinforced polymers. *Journal of Materials Science* **34**: 5513-5517.
5. Akay E., Yilmaz C., Kocaman E.S., Turkmen H.S. and Yildiz M. (2016) Monitoring Poisson's Ratio Degradation of FRP Composites under Fatigue Loading Using Biaxially Embedded FBG Sensors. *Materials* **9**: 15.
6. Amara K.H., Tounsi A. and Benzair A. (2005) Transverse cracking and elastic properties reduction in hygrothermal aged cross-ply laminates. *Materials Science and Engineering a-Structural Materials Properties Microstructure and Processing* **396**: 369-375.
7. Yilmaz C., Akalin C., Kocaman E.S., Suleman A. and Yildiz M. - Monitoring Poisson’s ratio of glass fiber reinforced composites as damage index using biaxial Fiber Bragg Grating sensors. **-** 98.
8. Melin L.N. and Neumeister J.M. (2006) Measuring constitutive shear behavior of orthotropic composites and evaluation of the modified Iosipescu test. *Composite Structures* **76**: 106-115.
9. Tew B.W., Odom E.M. and Teel J.D. (2001) Composite specimen bearing failure reduction in iosipescu shear tests. *Experimental Mechanics* **41**: 218-224.
10. Pierron F. and Vautrin A. (1998) Measurement of the in-plane shear strengths of unidirectional composites with the Iosipescu test. *Composites Science and Technology* **57**: 1653-1660.
11. Odegard G. and Kumosa M. (2000) Determination of shear strength of unidirectional composite materials with the Iosipescu and 10 degrees off-axis shear tests. *Composites Science and Technology* **60**: 2917-2943.
12. Han L. and Piggott M. (2002) Tension-compression and Iosipescu tests on laminates. *Composites Part a-Applied Science and Manufacturing* **33**: 35-42.
13. Pierron F. and Vautrin A. (1997) Measurement of the in-plane shear strengths of unidirectional composites with the Iosipescu test. *Composites Science and Technology* **57**: 1653-1660.
14. Sun Y.T., Shi D.Q., Yang X.G., Mi C.H., Feng J. and Jiang Y.G. (2013) Stress State Analysis of Iosipescu Shear Specimens for Aerogel Composite with Different Properties in Tension and Compression. *7th Asian-Pacific Conference on Aerospace Technology and Science, Apcats 2013* **67**: 517-524.
15. Salavatian M. and Smith L. (2014) The effect of transverse damage on the shear response of fiber reinforced laminates. *Composites Science and Technology* **95**: 44-49.
16. Salavatian M. and Smith L. (2014) An improved analytical model for shear modulus of fiber reinforced laminates with damage. *Composites Science and Technology* **105**: 9-14.
17. Li L., Lomov S.V. and Yan X. (2015) Correlation of acoustic emission with optically observed damage in a glass/epoxy woven laminate under tensile loading. *Composite Structures* **123**: 45-53.
18. Li L., Lomov S.V., Yan X. and Carvelli V. (2014) Cluster analysis of acoustic emission signals for 2D and 3D woven glass/epoxy composites. *Composite Structures* **116**: 286-299.
19. Carvelli V., D'Ettorre A. and Lomov S.V. (2017) Acoustic emission and damage mode correlation in textile reinforced PPS composites. *Composite Structures* **163**: 399-409.
20. Genest M., Martinez M., Mrad N., Renaud G. and Fahr A. (2009) Pulsed thermography for non-destructive evaluation and damage growth monitoring of bonded repairs. *Composite Structures* **88**: 112-120.
21. Liu C., Cheng L., Luan X., Li B. and Zhou J. (2008) Damage evolution and real-time non-

destructive evaluation of 2D carbon-fiber/SiC-matrix composites under fatigue loading. *Materials Letters* **62**: 3922-3924.

22. Naderi M., Kahirdeh A. and Khonsari M.M. (2012) Dissipated thermal energy and damage evolution of Glass/Epoxy using infrared thermography and acoustic emission. *Composites Part B: Engineering* **43**: 1613-1620.
23. Montesano J., Fawaz Z. and Bougherara H. (2015) Non-destructive assessment of the fatigue strength and damage progression of satin woven fiber reinforced polymer matrix composites. *Composites Part B: Engineering* **71**: 122-130.
24. Crupi V. (2008) An Unifying Approach to assess the structural strength. *International Journal of Fatigue* **30**: 1150-1159.
25. Fargione G., Geraci A., La Rosa G. and Risitano A. (2002) Rapid determination of the fatigue curve by the thermographic method. *International Journal of Fatigue* **24**: 11-19.
26. Grosse C.U. and Finck F. (2006) Quantitative evaluation of fracture processes in concrete using signal-based acoustic emission techniques. *Cement & Concrete Composites* **28**: 330-336.
27. Schubert E., Koos A., Emrich T., Züfle A., Schmid K.A. and Zimek A. (2015) A framework for clustering uncertain data. *Proceedings of the VLDB Endowment* **8**: 1976-1979.
28. Kempf M., Skrabala O. and Altstadt V. (2014) Acoustic emission analysis for characterisation of damage mechanisms in fibre reinforced thermosetting polyurethane and epoxy. *Composites Part B-Engineering* **56**: 477-483.
29. Yilmaz C. and Yildiz M. (2017) A study on correlating reduction in Poisson's ratio with transverse crack and delamination through acoustic emission signals. *Polymer Testing* **63**: 47-53.
30. Kocaman E., Akay E., Yilmaz C., Turkmen H., Misirlioglu I., Suleman A. and Yildiz M. (2017) Monitoring the Damage State of Fiber Reinforced Composites Using an FBG Network for Failure Prediction. *Materials* **10**.
31. Hausrath R.L. and Longobardo A.V. (2010) High-strength glass fibers and markets. In: Fiberglass and Glass Technology. Springer: 197-225.